In-Situ Spectroscopic Ellipsometry for Thermochromic $CsPbI_3$ Phase Evolution Portfolio

Meng Yuan[†], Long Yuan[†]*, Zhiyan Hu[†], Zhaoliang Yu[†], Haibo Li[†,]*, Eva M. Barea[‡], Juan Bisquert[‡], Xiangdong Meng[† §] *

[†]Key Laboratory of Functional Materials Physics and Chemistry of the Ministry of Education, Jilin Normal University, Changchun, P. R. China. X.M. email: mengxiangdong@jlnu.edu.cn; L.Y. email: yuanlong@jlnu.edu.cn; H.L. lihaibo@jlnu.edu.cn

[‡]Institute of Advanced Materials (INAM), Universitat Jaume I, 12006 Castelló, Spain.

[§] Key Laboratory of Preparation and Application of Environmental Friendly Materials, Ministry of Education, Jilin Normal University, Changchun 130103, P. R. China.

Contents

Appendix

Tauc-Lorentz model

This model is from Jellison and Modine, APL 69,371-373 (1996). In this original paper, there is an error of calculation of the real part of the dielectric function.

In the Tauc-Lorentz model, the ε_2 is expressed as a product of the Tauc gap and the Lorentz model:

$$\varepsilon = \varepsilon_1 + i\varepsilon_2$$

$$i\varepsilon_2 = \begin{cases} \dfrac{1}{E} \cdot \dfrac{\mathrm{A} \cdot \mathrm{E}_0 \cdot \mathrm{C} \cdot (\mathrm{E} - \mathrm{E}_g)^2}{2a} & (E > E_g) \\ 0 & (E \le E_g) \end{cases}$$

$$\varepsilon_1 = \frac{\pi}{2} \cdot P \cdot \int_{E_g}^{\infty} \frac{\xi \cdot \varepsilon_2(\xi)}{\xi^2 - E^2}$$

where A is the amplitude parameter, C is the broadening parameter, and $\mathrm{E_o}$ represents the peak transition energy. The corresponding ε_1 is obtained from ε_2 by the Kramers–Kronig relations.

Solving the integral:

$$\varepsilon_1 = \frac{A \cdot C \cdot a_{\ln}}{2 \cdot \pi \cdot \xi^4 \cdot \alpha \cdot E_0} \cdot \ln\left[\frac{E_0^2 + E_g^2 + \alpha \cdot E_g}{E_0^2 + E_g^2 - \alpha \cdot E_g}\right] - \frac{A \cdot a_{a \cdot \tan}}{\pi \cdot \xi^4 \cdot E_0}$$
$$\cdot \left[\pi - a \cdot \tan\left(\frac{2 \cdot E_g + \alpha}{C}\right) + a \cdot \tan\left(\frac{\alpha - 2 \cdot E_g}{C}\right)\right] + \frac{2 \cdot A \cdot E_0}{\pi \cdot \xi^4 \cdot \alpha}\left\{E_g \cdot (E^2 - \gamma^2) \cdot \left[\pi + 2 \cdot a\right.\right.$$
$$\left.\left. \cdot \tan\left(\frac{\gamma^2 - E_g^2}{\alpha \cdot C}\right)\right]\right\} - \frac{A \cdot E_0 \cdot C \cdot (E^2 + E_g^2)}{\pi \cdot \xi^4 \cdot E}$$
$$\cdot \ln\left(\frac{|E - E_g|}{E + E_g}\right) + \frac{2 \cdot A \cdot E_0 \cdot C \cdot E_g}{\pi \cdot \xi^4} \cdot \ln\left[\frac{|E - E_g| \cdot (E + E_g)}{\sqrt{(E_0^2 - E_g^2)^2 + E_g^2 \cdot C^2}}\right]$$

where:

$$a_{\ln} = (E_g^2 - E_0^2)E^2 + E_g^2 C^2 - E_0^2(E_0^2 + 3E_g^2)$$

$$a_{a \cdot \tan} = (E^2 - E_0^2)(E_0^2 + E_g^2) + E_g^2 C^2$$

$$\xi^4 = (E^2 - \gamma^2)^2 + \frac{\alpha^2 \cdot C^2}{4}$$

$$\alpha = \sqrt{4 \cdot E_0^2 - C^2}$$

$$\gamma = \sqrt{4 \cdot E_0^2 - \frac{C^2}{2}}$$

In the actual calculation, the values of $|E - E_g|$ were chosen to not become zero. Therefore, the Tau–Lorentz model is determined by five parameters [ε_1, A, C, E_g and E_0.]

$$\mathrm{E}(eV) = h\upsilon = \frac{1240}{\lambda(nm)}$$

$$\alpha(\lambda) = \frac{4\pi k(\lambda)}{\lambda}$$

The relationship between complex optical constant and complex dielectric constant:

$$\tilde{\mathrm{N}} = \mathrm{n} - \mathrm{ik}$$

$$\varepsilon = \varepsilon_1 - i\varepsilon_2$$

$$\varepsilon = \tilde{\mathrm{N}}^2$$

$$n^2 - k^2 = \varepsilon_1$$

$$2\mathrm{nk} = \varepsilon_2$$

Theoretical spectrum is adjusted to experimental one. Goodness of fit is given by value χ^2. It should be as small as possible:

$$\chi^2 = min\sum_{i=1}^{n}\left[\frac{(\Psi_{th} - \Psi_{exp})_i^2}{\Gamma_{\Psi,i}} + \frac{(\Delta_{th} - \Delta_{exp})_i^2}{\Gamma_{\Delta,i}}\right]$$

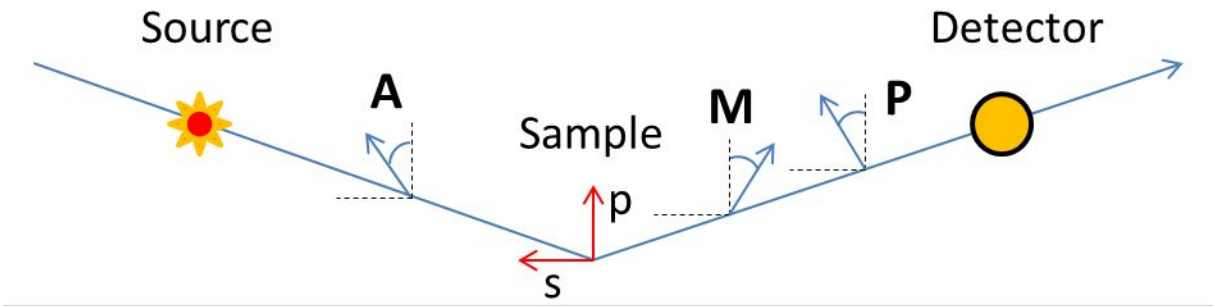

Detected electric field is deduced through Jones matrix product and incident electric field Jones vector：

$$\overrightarrow{E_d} = [AR_A SR_M MR_{P-M} P]\overrightarrow{E_i}$$

Only intensity is measurable, proportional to square of field.

$$\mathrm{I} = \left|\overrightarrow{E_d}\right|^2 = I_O + I_S \sin\delta(t) + I_C \cos\delta(t)$$

In the general case for P, M, and A:

$$I_O = 1 - \cos 2\Psi \cos A + \cos 2(P-M)\cos 2M(\cos 2A - \cos 2\Psi) + \cos 2(P-M)\sin 2A \sin 2M \sin 2\Psi \cos\Delta$$

$$I_S = \sin 2(P-M)\sin 2A \sin 2\Psi \sin\Delta$$

$$I_C = \sin 2(P-M)[\sin 2M(\cos 2\Psi - \cos 2A) + \sin 2A \cos 2M \sin 2\Psi \cos\Delta]$$

By construction P-M = 45^o , then I_S I_C relation to Ψ and Δ becomes simple:

$$\mathrm{M} = 0^o \pm 90^o \text{ and } \mathrm{A} = \pm 45^O, \text{ then}$$

$$I_S = \pm_A \sin 2\Psi \sin\Delta \text{ and } I_C = \pm_M \pm_A \sin 2\Psi \cos\Delta$$

In this work, we use that Configuration Ⅱ : P – M = $45^o[90^o]$; M=$0^o[90^o]$; A=$45^o[90^o]$

$$I_S = \sin 2\Psi \sin\Delta \text{ and } I_C = \cos 2\Psi$$

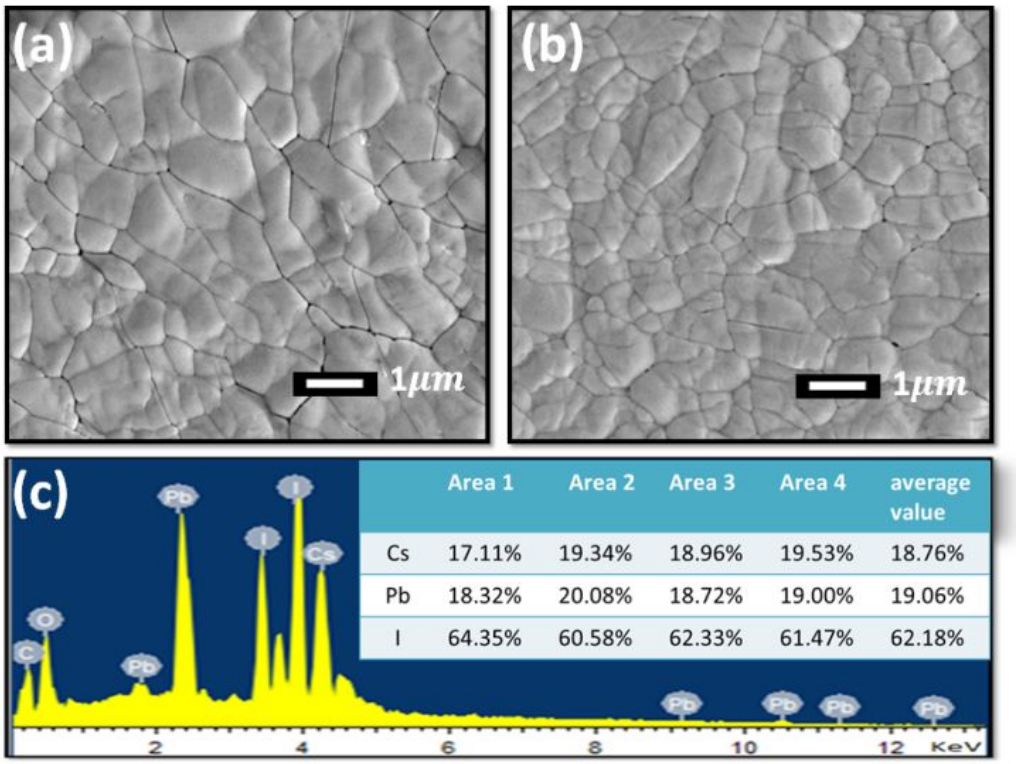

	Area 1	Area 2	Area 3	Area 4	average value
Cs	17.11%	19.34%	18.96%	19.53%	18.76%
Pb	18.32%	20.08%	18.72%	19.00%	19.06%
I	64.35%	60.58%	62.33%	61.47%	62.18%

Figure S1 (a) SEM image of the δ-$CsPbI_3$ after once or twice (b) conversion between high and low temperature phase. (c) EDS of the δ-$CsPbI_3$ and the inset table is the percentage of element content in five different points.

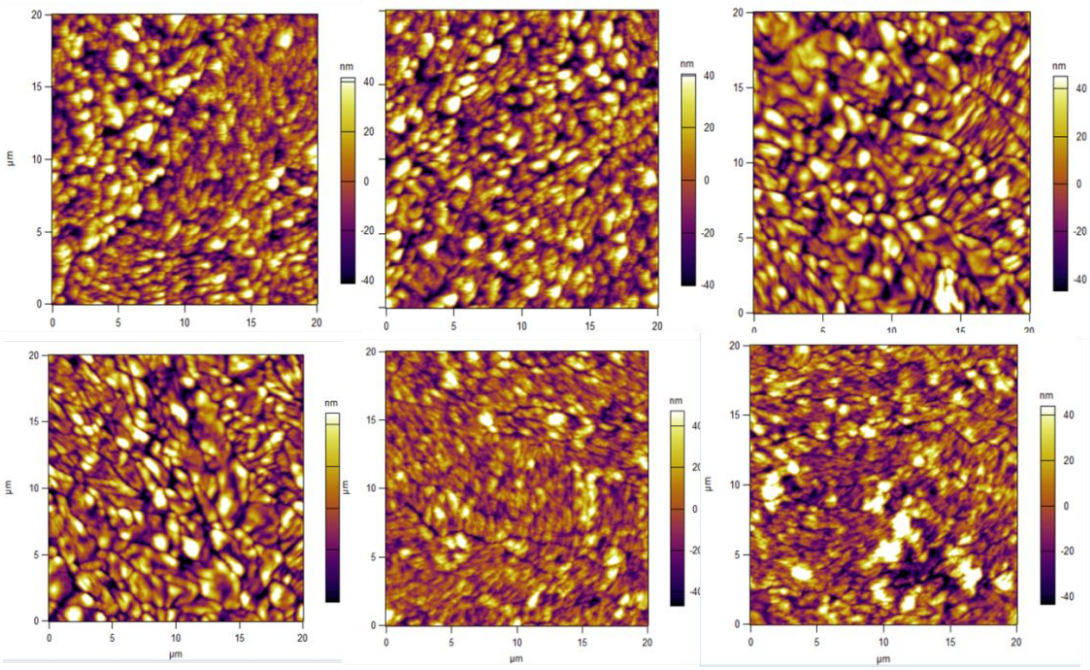

Figure S2 Atomic force micrographs of the δ-$CsPbI_3$ thin films.

Table S1 Roughness and average value of the above six δ-$CsPbI_3$ samples.

	RMS (nm)	Max (nm)	Min (nm)
Area1	19.085	85.149	-73.508
Area2	20.434	81.849	-70.881
Area3	22.965	123.020	-76.865
Area4	22.770	102.695	-83.505
Area5	17.238	88.743	-63.286
Area6	21.218	114.505	-72.673
average value	20.618	99.327	-73.453

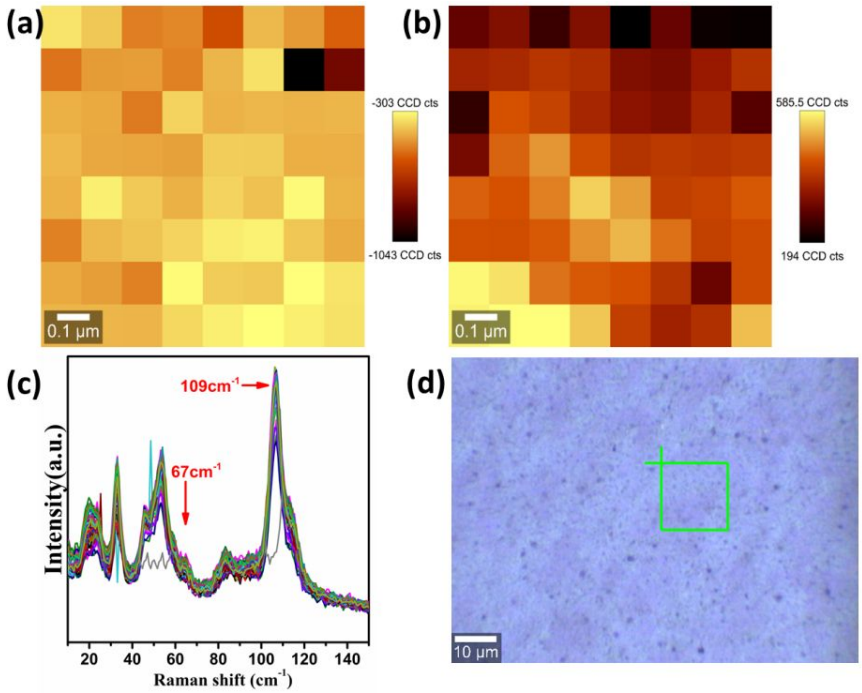

Figure S3 The α-$CsPbI_3$ thin films photography of in situ confocal low frequency Raman spectra at (a) 53 cm^{-1} and (b) 106 cm^{-1}. (c) is spectrums of in situ confocal Raman, and the characteristic peak position is marked by arrow. (d) is a microscopic photograph of the test point.

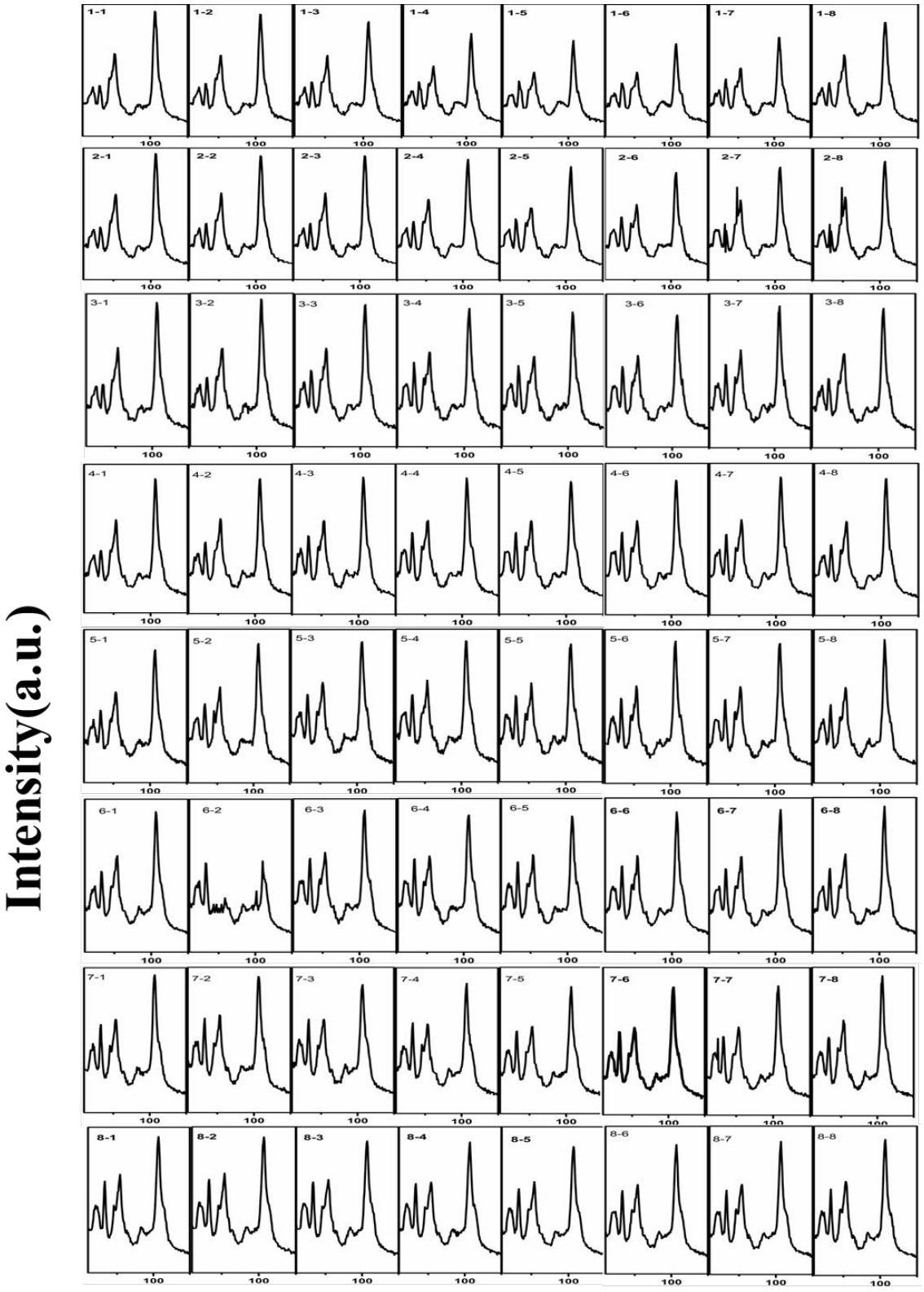

Figure S4 The in situ confocal Raman spectra of the δ-$CsPbI_3$ thin films at each point (resolution: 0.1*0.1 μm^2).

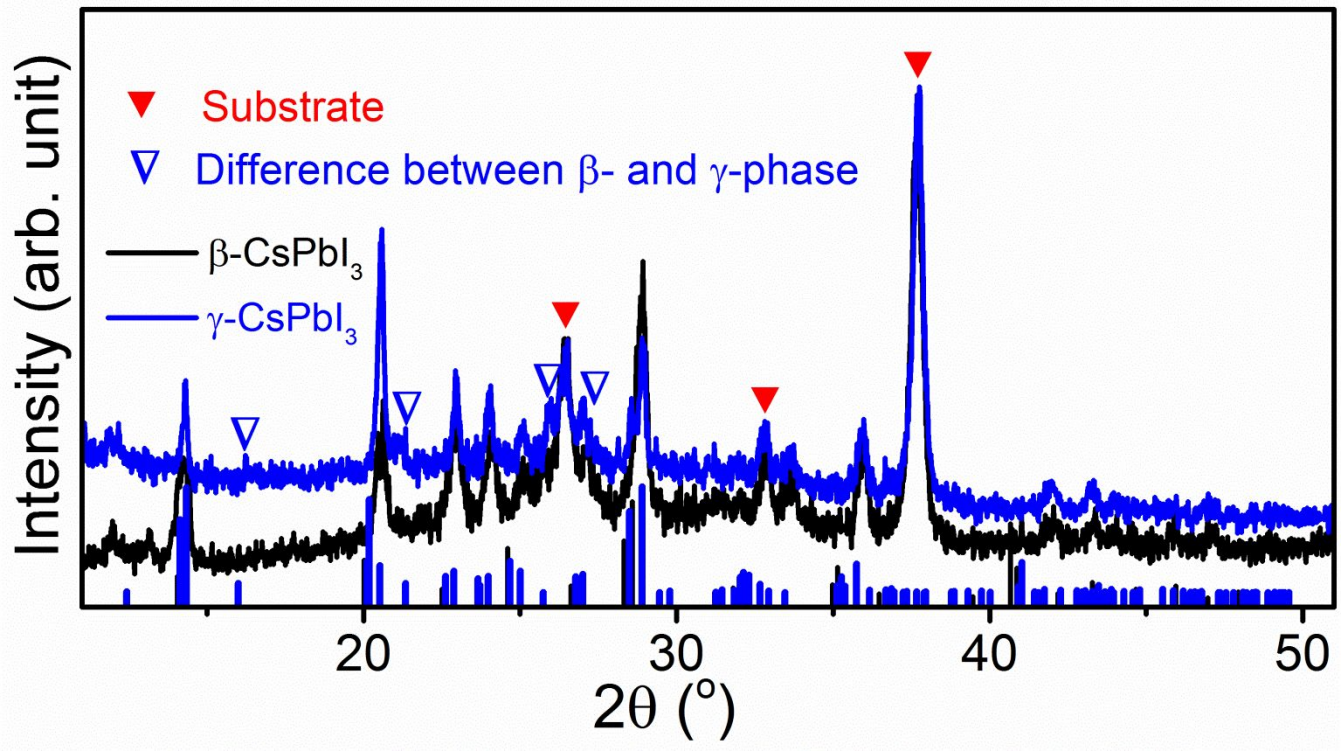

Figure S5 Comparison of the XRD difference of β- and γ-$CsPbI_3$ film.

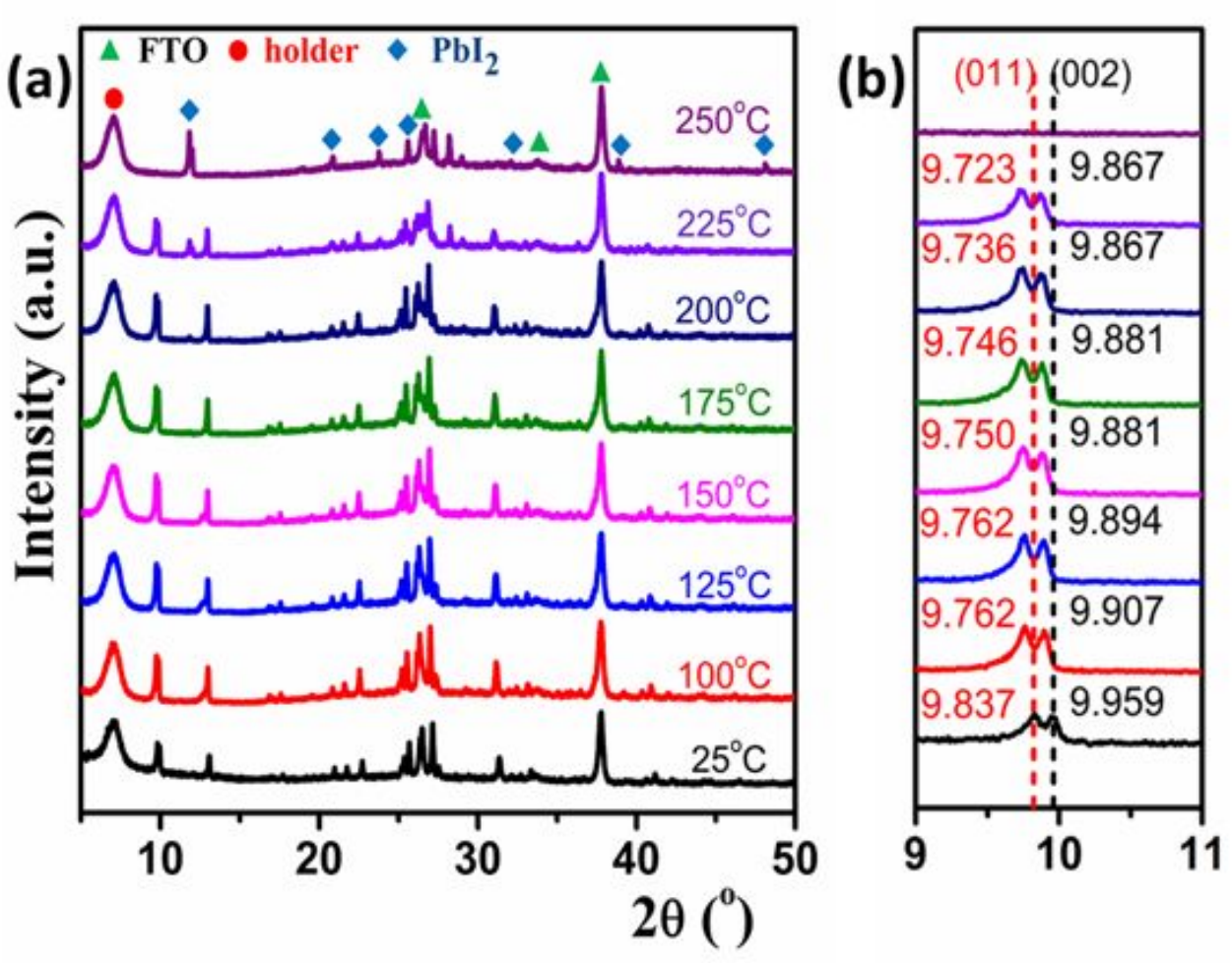

Figure S6 (a) Temperature dependent XRD of $CsPbI_3$ film measured in vacuum and enlarged view of the diffraction results in the 2-theta range of 9-11 °C.

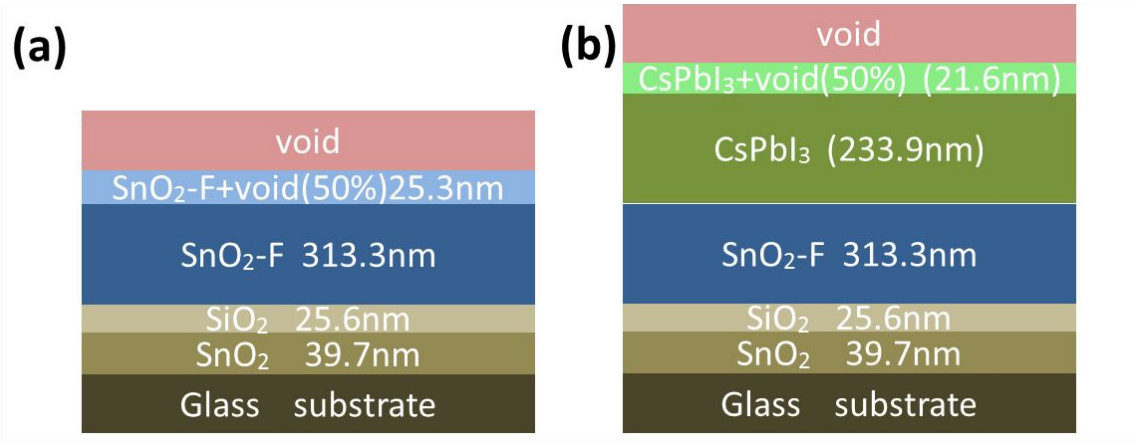

Figure S7 Schematics of the optical model of (a) the FTO substrate and (b) the $CsPbI_3$ thin films.

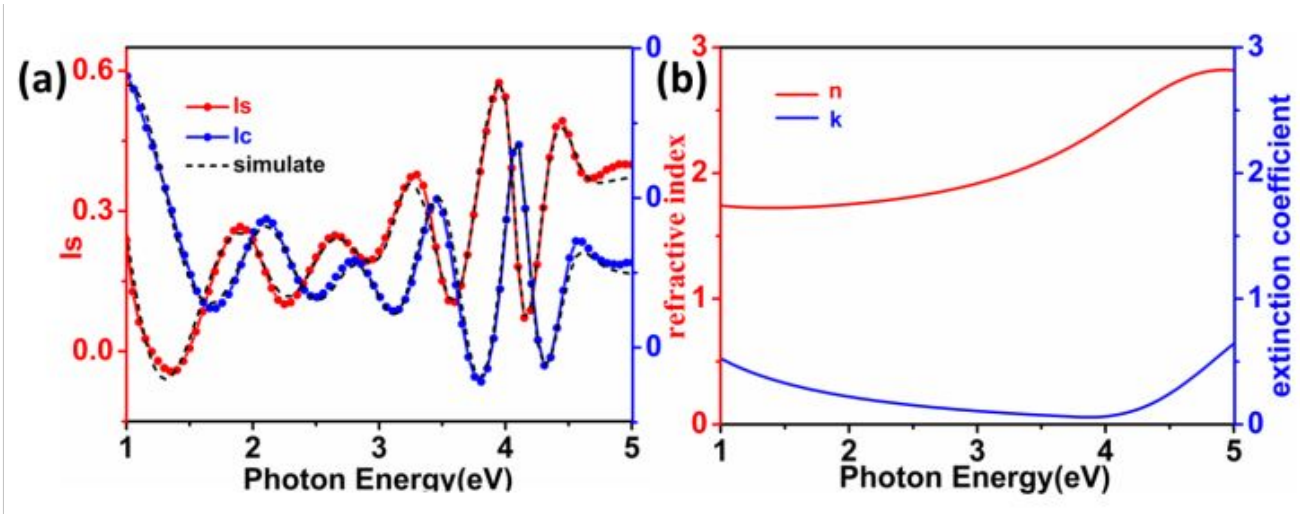

Figure S8 Measurement and analysis for the FTO substrate: (a) Ellipsometric experimental spectra (point lines) and simulate spectra (dotted lines) of the FTO substrate at a 70 ° angle of incidence. (b) Photo energy-dependent optical constants of the FTO layer.

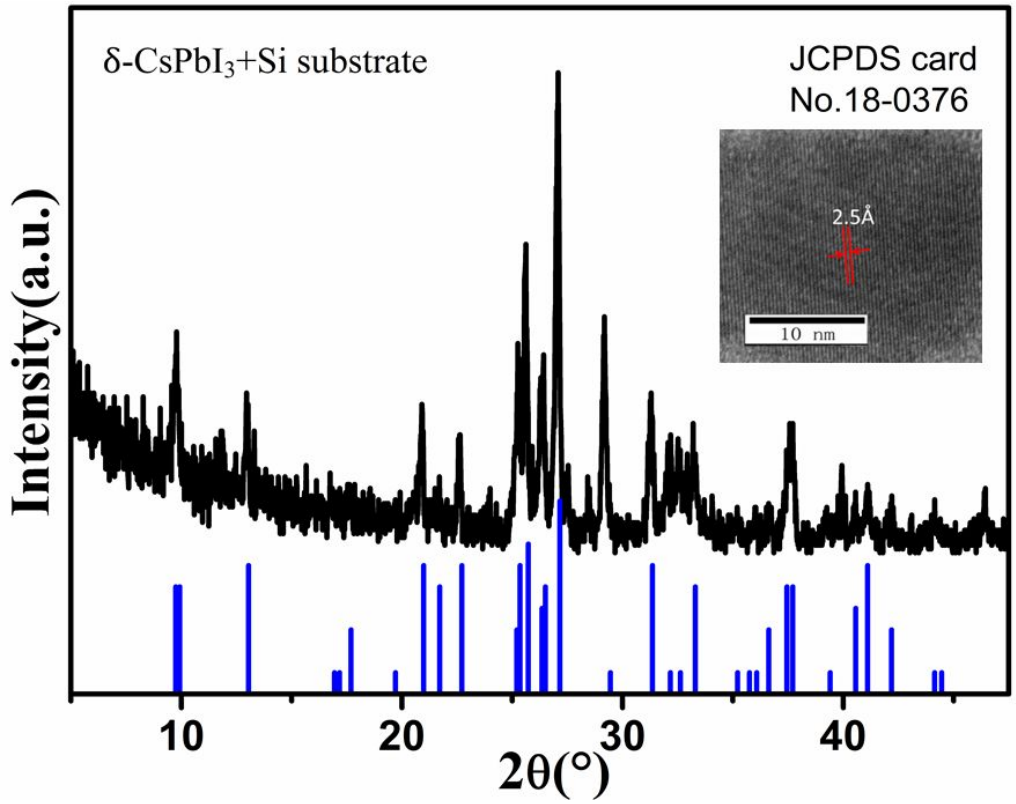

Figure S9 XRD patterns of the δ-$CsPbI_3$ thin film on silicon substrate. Inset shows a HRTEM image of δ-$CsPbI_3$ with a lattice fringe of 2.5 Å.

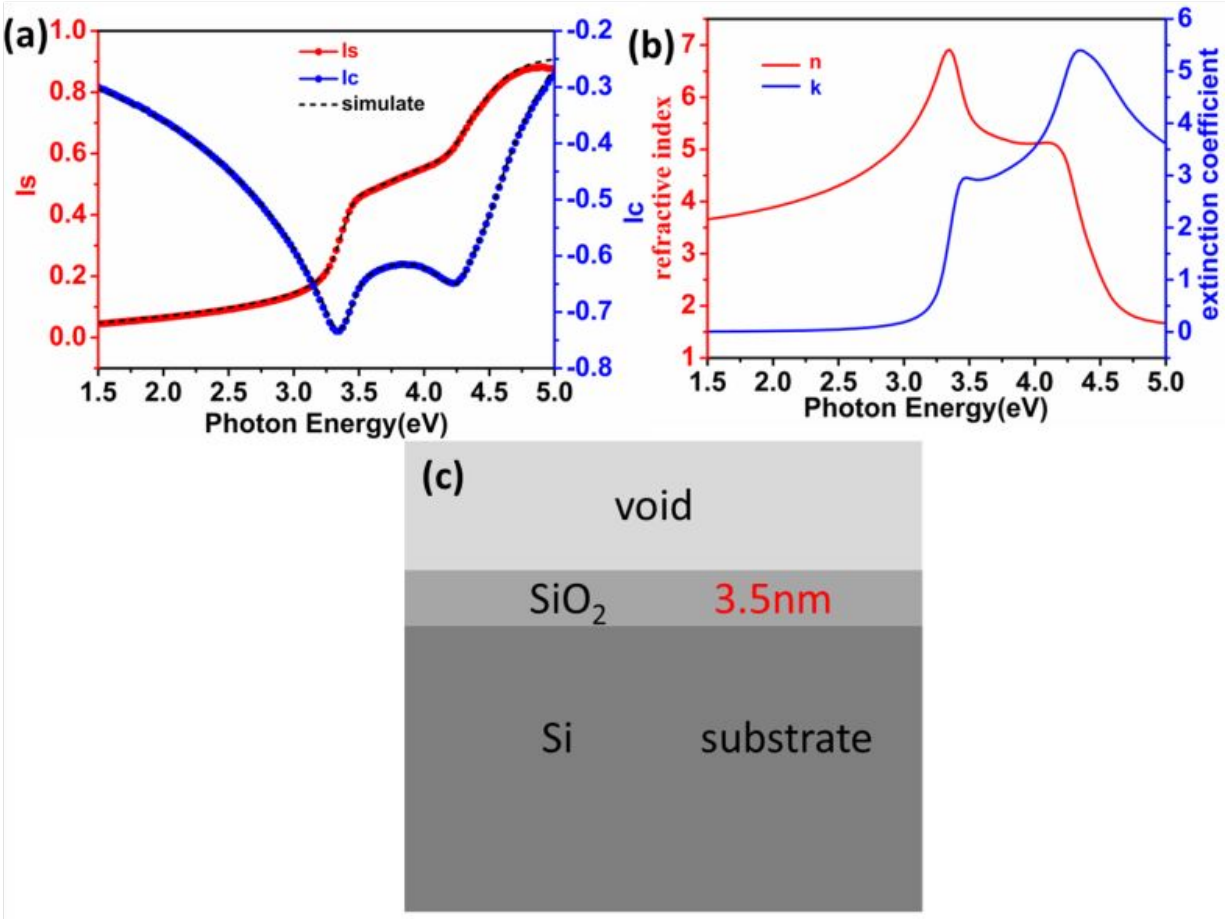

Figure S10 Measurement and analysis for the Si substrate: (a) Ellipsometric experimental spectra (point lines) and simulate spectra (dotted lines) of the Si substrate at a 70 ° angle of incidence. (b) Photon energy-dependent optical constants of the SiO_2 layer. (c) Schematic of the optical model. Results of the fitting parameters are marked in red in the model.

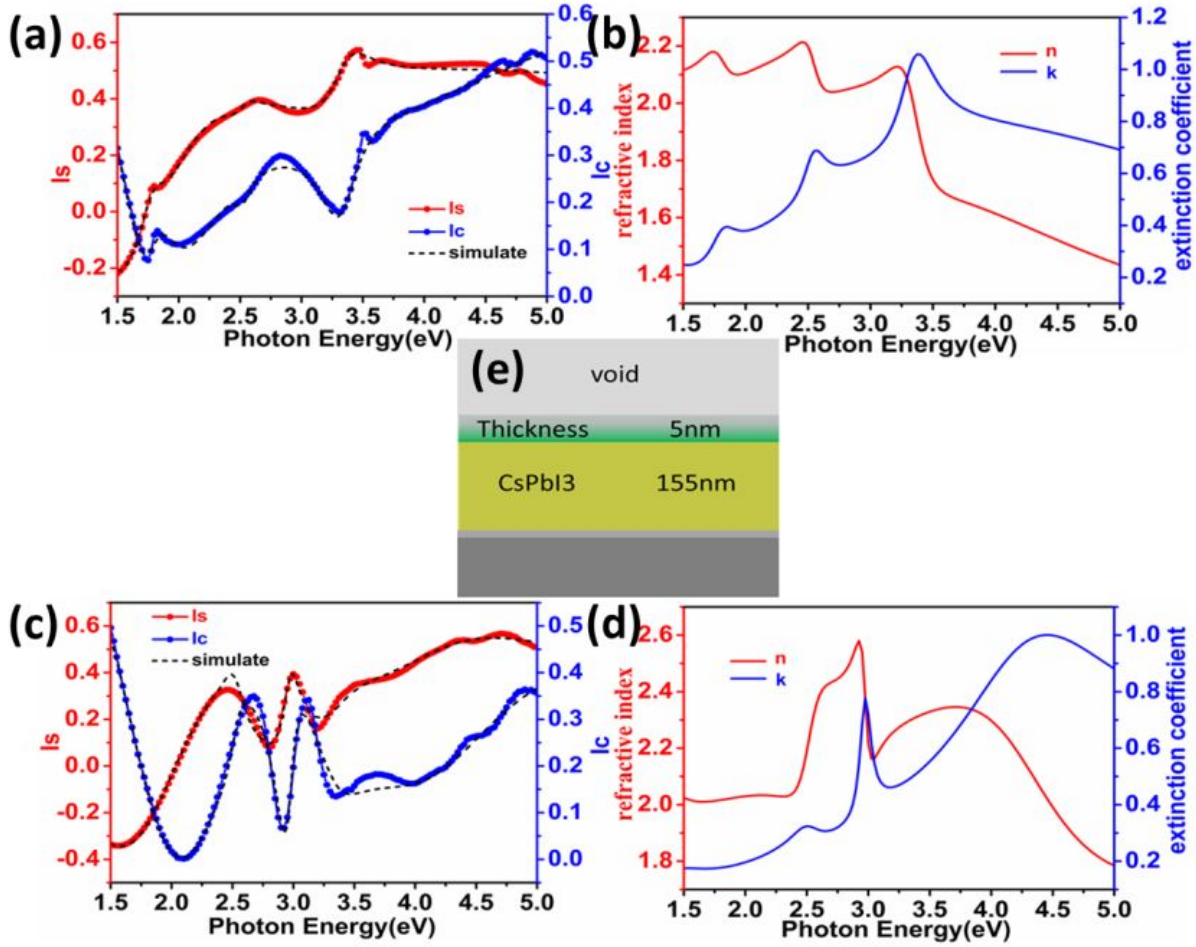

Figure S11 Measurement and analysis for the α-$CsPbI_3$ and the δ-$CsPbI_3$ thin film on the Si substrate: (a) and (c) Ellipsometric experimental spectra (point lines) and simulate spectra (dotted lines) of the α-$CsPbI_3$ and the δ-$CsPbI_3$ thin film at a 70 ° angle of incidence. (b) and (d) Photo Energy-dependent optical constants of the α-$CsPbI_3$ and the δ-$CsPbI_3$ thin film layer.(e) Schematic of the optical model.

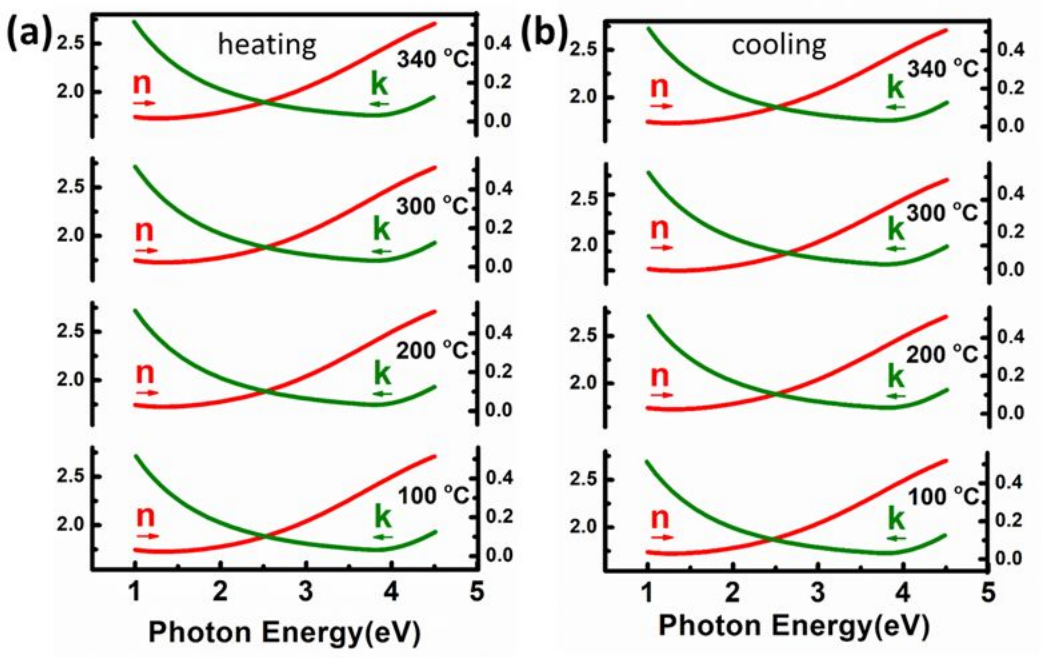

Figure S12 In-situ dynamic ellipsometry spectra of FTO substrate in (a) heating and (b) cooling processes from 100 to 360 °C.

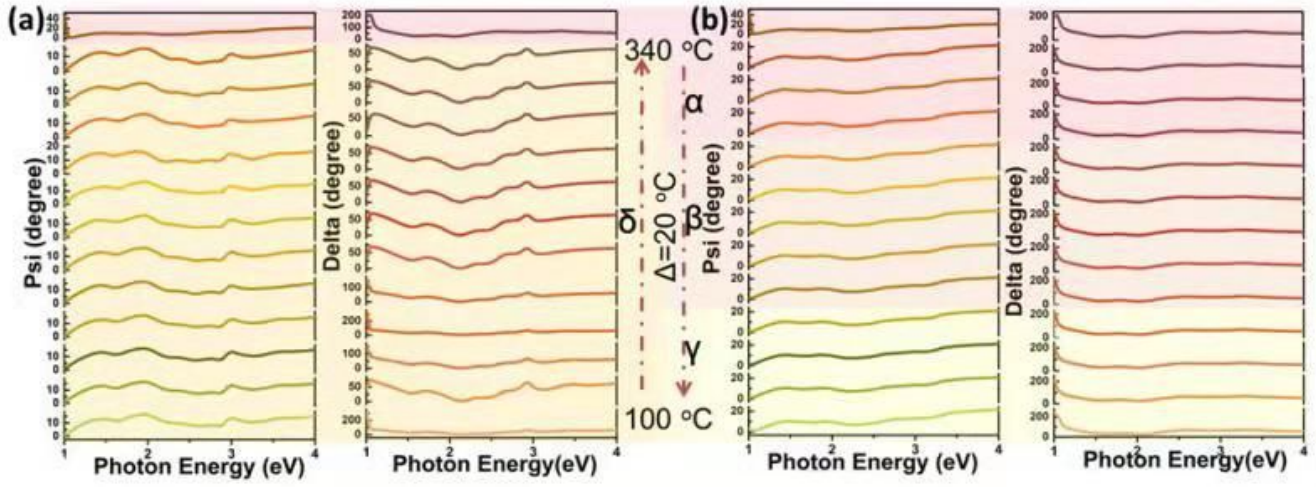

Figure S13 In-situ dynamic ellipsometry spectra of as-prepared $CsPbI_3$ film in (a) heating and (b) cooling processes from 100 to 360 °C.

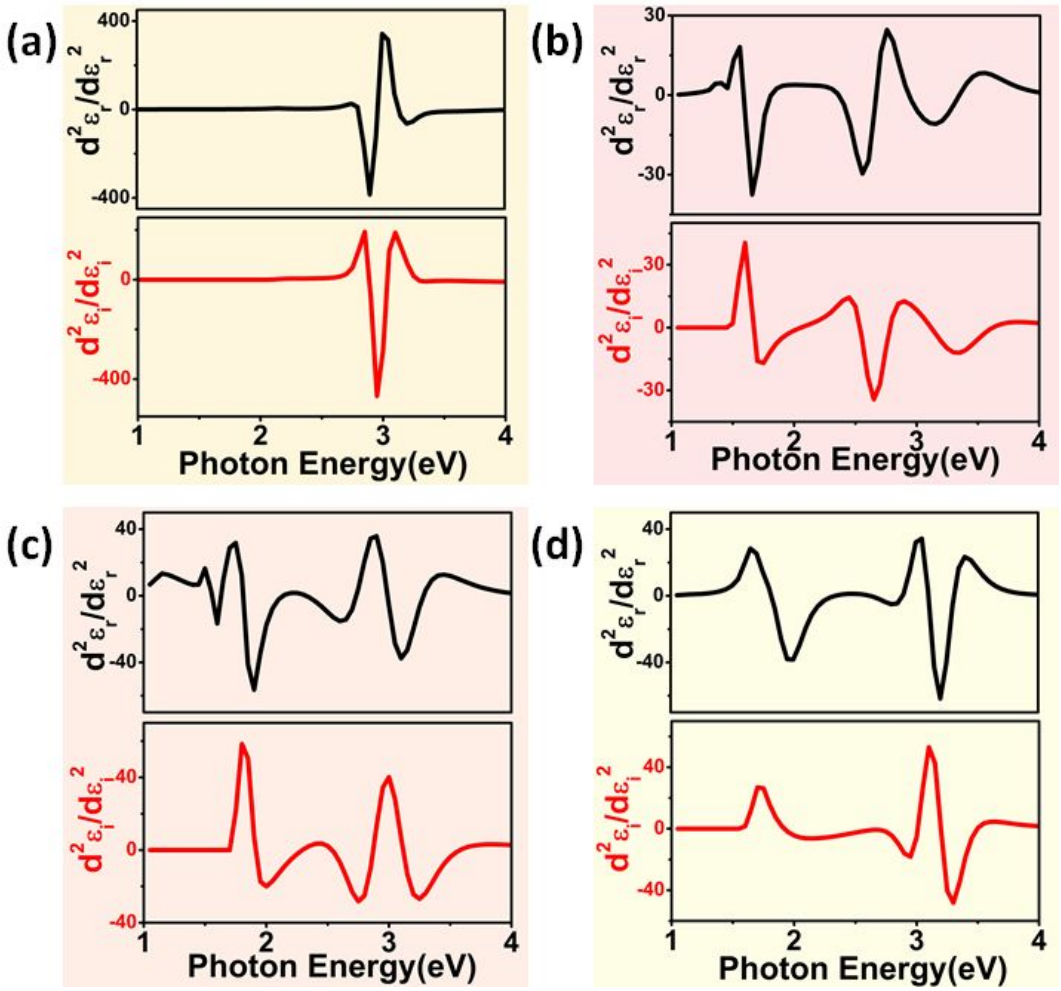

Figure S14 Second derivatives of the pseudodielectric function numerically calculated spectra for four phases of $CsPbI_3$ thin films: (a) δ (b) α, (c) β and (d) γ, respectively.